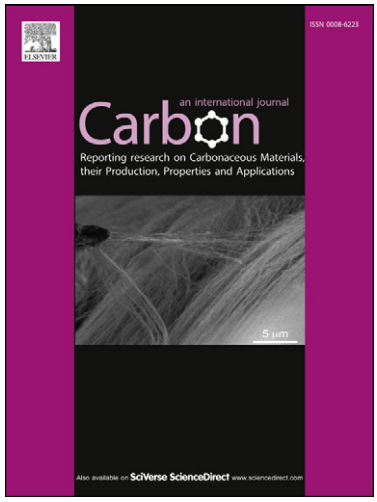

Synthesis and Analysis of Thin Conducting Pyrolytic Carbon Films

Niall McEvoy, Nikolaos Peltekis, Shishir Kumar, Ehsan Rezvani, Hugo Nolan, Gareth P. Keeley, Werner J. Blau, Georg S. Duesberg

PII: S0008-6223(11)00866-9
DOI: 10.1016/j.carbon.2011.10.036
Reference: CARBON 6904

To appear in: *Carbon*

Received Date: 13 July 2011
Accepted Date: 20 October 2011

Please cite this article as: McEvoy, N., Peltekis, N., Kumar, S., Rezvani, E., Nolan, H., Keeley, G.P., Blau, W.J., Duesberg, G.S., Synthesis and Analysis of Thin Conducting Pyrolytic Carbon Films, *Carbon* (2011), doi: 10.1016/j.carbon.2011.10.036

Synthesis and Analysis of Thin Conducting Pyrolytic Carbon Films

Niall McEvoy[1], Nikolaos Peltekis[1], Shishir Kumar[1, 2], Ehsan Rezvani[1, 2], Hugo Nolan[1, 2], Gareth P. Keeley[1, 2, 3], Werner J. Blau[1, 4], Georg S. Duesberg[1, 2]*

[1] *CRANN, Trinity College Dublin, Dublin 2, Ireland*

[2] *School of Chemistry, Trinity College Dublin, Dublin 2, Ireland*

[3] *Département de Chimie Moléculaire, UMR 5250, ICMG FR 2607, CNRS, Université Joseph Fourier, BP 53, 38041 Grenoble cedex 9, France*

[4] *School of Physics, Trinity College Dublin, Dublin 2, Ireland*

Abstract

We report on an adjustable process for chemical vapour deposition of thin films of pyrolytic carbon on inert substrates using an acetylene feedstock. Through modification of the reaction parameters control over film thickness and roughness is attained. These conducting films can be deposited in a conformal fashion, with thicknesses as low as 5 nm and a surface roughness of less than 1 nm. The highly reliable, cost effective and scalable synthesis may have a range of applications in information and communications technology and other areas. Raman and X-ray photoelectron spectroscopies, as well as high resolution transmission electron microscopy are used to investigate the composition and crystallinity of these films. The suitability of these films as electrodes in transparent conductors is assessed through a combination of absorbance and sheet resistance measurements. The films have a resistivity of ~ 2×10^{-5} Ωm but absorb strongly in the visible range. The electrochemical properties of the films are investigated and are seen to undergo a marked improvement following exposure to O_2 or N_2 plasmas, making them of interest as electrochemical electrodes.

*Corresponding author. Tel/Fax: +353 (1)896 3035. E-mail address: duesberg@tcd.ie (G.S. Duesberg)

1. Introduction

Nanocarbon materials, including carbon nanotubes (CNTs) and graphene display favourable electrical and chemical properties and have garnered much attention from the research community. In particular, many researchers have attempted to exploit the high conductivity of CNTs and graphene for transparent electrodes for display[1, 2], energy[3] and sensing[4] applications. The high conductivities of thin films of these materials make them promising candidates for replacing the increasingly scarce indium tin oxide (ITO) as the industry standard material in transparent electrodes. Further, carbon based materials have long been used as electrochemical electrodes for sensing and energy applications. Such materials possess large potential windows and high electrochemical stability. However, purpose synthesised graphite electrodes (edge cut HOPG) are high in cost and difficult to process.

Whilst the properties of CNTs are highly impressive, CNT devices currently suffer from relatively inefficient processing and contacting processes. A similar argument holds true for graphene, where the best performing materials are still produced by mechanical exfoliation, despite the recent advances in scalability and throughput afforded by SiC decomposition[5], liquid phase exfoliation[6-8] and growth by chemical vapour deposition (CVD) on metal substrates[9-11].

With many unanswered questions pertaining to the manufacturability of CNTs and graphene, little attention has been given to thin films of pyrolytic carbon (PyC) for applications in information and communications technology (ICT) and electrochemistry. PyC is a disordered nanocrystalline graphitic material which can be formed through gas phase dehydrogenation (or pyrolysis) of hydrocarbons and subsequent deposition on surfaces. PyC belongs to the family of turbostratic carbons due to slipped or randomly oriented basal planes of crystallites.

The lack of need for a catalyst and reaction-limited gas phase deposition allow for conformal coatings on a variety of substrates. Infiltration of porous materials and fibres is also possible.

PyC exhibits good thermal and electrical conductivity as well as high durability and chemical and wear resistance. The thermal and mechanical properties have led to usage as a coating for individual pebbles in pebble bed reactors[12] and rocket nozzles[13] as well as electronic thermal management applications including heat spreaders[14]. PyC is biocompatible and thromboresistant and has been investigated as a coating for heart valves and other forms of prosthesis [15, 16]. Chemical vapour infiltration (CVI) has been used with CNFs to form assorted carbon felt materials [17-19]. It has also been used to coat optical fibres making them more resistant to harsh environmental conditions[20]. Conformal deposition into pores and trenches also allows for the usage of PyC as a liner for trench capacitors in dynamic random-access memory (DRAM) devices[21]. PyC can be readily patterned making it suitable for other microelectronics components including vertical interconnects (VIAS) and wires[22], gate electrodes[23] and electrodes in metal-silicon-insulator (MSI) capacitors[24]. The ease of processing and favourable properties mark PyC as a promising candidate for novel approaches to device fabrication[25].

The pyrolysis of hydrocarbons is a complex process with a large number of different reaction pathways. The chemistry and kinetics of PyC formation from different hydrocarbons has been extensively investigated by a number of groups. The Tesner group investigated the formation of PyC from different precursors. In the case of acetylene they established that at temperatures below 1000 ^{o}C the rate of formation of pyrolytic carbon was proportional to the acetylene concentration with a well-defined rate constant[26]. At higher temperatures contributions from the products of decomposition of acetylene made kinetic measurements more complicated. The Huttinger group also performed detailed studies on the pyrolysis of different hydrocarbons [27-31]. In the case of acetylene[27], it was shown to be very reactive

in PyC deposition and that ethylene, benzene and methane were all formed upon pyrolysis but at low partial pressures, thus suggesting direct deposition from C_2H_2. Higher deposition rates were observed with longer reaction times indicating the formation of consecutive products with higher reactivity after a short period of time (0.11 - 0.33 s) at a temperature of 1000 ^{o}C. In recent years the Marquaire group have researched the deposition of PyC from propane. Over the course of this the gas phase species involved were identified and kinetic models proposed [32, 33]. Furthermore, the influence of reactor geometry, deposition temperature and residence time on the deposition rate of PyC was detailed [34, 35].

This paper reports on the production of thin films of PyC on assorted inert substrates by CVD. The effect of varying growth parameters was investigated in order to achieve fine control over the thickness, conformality, sheet resistance and roughness of the films grown. The electrical properties of the films grown are compared with state of the art thin films and their use in high-tech applications including transparent conductors and electrochemical electrodes is assessed.

The films produced were extensively characterised using various forms of spectroscopy and microscopy giving information on the composition and crystallinity of the films. Atomic force microscopy (AFM) was used to probe the surface of films grown, demonstrating their smooth nature. High-resolution transmission electron microscopy (HRTEM) analysis was used to image crystalline domains complimenting the Raman analysis.

2. Experimental Setup

2.1 Sample Preparation

PyC films were grown in a Gero quartz tube furnace (700 x 90 mm) using acetylene (C_2H_2, BOC, minimum 98.5% purity) as the hydrocarbon feedstock at a flow rate of 180 sccm.

Temperatures in the range 850 – 1100 ^{o}C were employed with pressures in the range 5 – 20 Torr. The reaction chamber was evacuated to a pressure of < 5 mTorr before the introduction of acetylene. SiO_2 (300 nm) films on Si <100> were used as the primary growth substrates. Wafers (Si-Mat) were diced into substrates ~ 1 cm^2 in area. No additional cleaning steps were used. Fused quartz substrates were used for transmittance measurements.

2.2 Thickness and Morphology Characterisation

Film thicknesses were measured by stylus profilometry (Dektak 6M, Veeco Instruments). A surgical blade was used to gently scratch the films, exposing the underlying SiO_2 without damaging it and the thickness was then measured in at least five regions per sample.

A Digital Instruments multimode scanning probe microscope with a Nanoscope IIIa controller was used for AFM analysis. This was operated in tapping mode to probe the surface roughness and morphology of PyC films. The probes used were fabricated from Si and consisted of a cantilever 125 μm in length with a resonant frequency of 320 kHz. The tip had a height of 10 μm and a radius < 8 nm. Processing software allowed for the calculation of the average (*Ra)* and the root mean square (*Rq)* roughness of films.

2.3 Electron Microscopy

Scanning electron microscopy (SEM) analysis was carried out using a Zeiss Ultra Plus FE SEM. Cross sectional images were attained by tilting the sample stage to 45^{o} and imaging from the side of films. An accelerating voltage of 2 kV was used with an in-lens detection system.

HRTEM studies were performed on cross sections of PyC on SiO_2 prepared in a Zeiss Auriga Focused Ion Beam (FIB) with a Cobra ion column. A reactive gas injection system was used for reactive ion etching and deposition of a Pt capping layer. These cross sections were

imaged at 300 kV using an FEI Titan 80-300 (S)TEM equipped with an S-TWIN objective lens and a high brightness (X-FEG) Schottky field emission gun with monochromator.

2.4 Spectroscopic Analysis

Raman spectra were taken with a Jobin Yvon Labram HR with an excitation wavelength of 632.8 nm. This had maximum power of 12 mW and was used with a diffraction grating with 600 lines/mm. A 100x long working distance objective lens was used giving a spatial resolution of 3 – 5 μm. Typically 5 spectra were taken for each sample to ensure uniformity.

XPS analysis was performed using an Omicron ESCA system with an EA 125 Analyser and XM1000MK II monochromatic X-ray source. The Al *Kα* X-ray source gave a 2 mm X-ray spot. The analyser was operated with a pass energy (*Ep*) of 50 eV for wide scans and 20 eV for fine scans leading to an instrumental resolution of ~1.25 eV wide scans and 0.65 eV for fine scans.

2.5 Resistance and Transmittance Measurements

The sheet resistance of PyC films was measured using a four point probe head (Jandel) connected to a Keithley 2400 sourcemeter. The sheet resistance *Rs* is given by the formula; $Rs = (V/I) \times CF$, where *CF* is a correction factor which depends on the dimensions of the sample being probed and the inter-probe spacing. For samples with thicknesses much less than the spacing between probes and lateral dimensions much larger than the spacing between probes a correction factor of (π /ln2) is suitable[36].

Absorbance measurements were carried out on PyC films grown on fused quartz substrates using a Cary Varian 6000i UV-Vis-NIR spectrometer. This gave information on the portion of light absorbed in the range 200 – 1800 nm. The portion of light transmitted at 550 nm was taken as the transmittance in the visible range.

2.6 Plasma Treatment and Electrochemical Analysis

Plasma treatments were performed using a R^3T TWR-2000T microwave radical generator. Experimental conditions involved an output power of 1 kW, gas flow rates of 20 sccm, exposure times of 10 minutes and a pressure of 0.2 Torr.

Electrochemical analysis was performed using a Gamry Ref 600 potentiostat with a 3 electrode configuration. Platinum wire and Ag/AgCl were used as counter and reference electrodes respectively. PyC films were mounted into a custom built holder whereby a nitrile O ring defined the region of the electrode exposed to the electrolyte (radius = 1.5 mm, as described elsewhere [37]).

3. Results and Discussion

3.1 CVD Growth

PyC films were grown on SiO_2 on Si <100> substrates (typically 1 cm^2 in area) at temperatures in the range of 850 – 1100 ^oC, using different deposition times, whilst keeping all other growth parameters constant (P = 20 Torr, flow = 180 sccm). For films grown at 950 ^oC and 20 Torr an increase in film thickness with increasing deposition time was evident from optical inspection (see Figure 1). Profilometry measurements indicated that this increase in thickness with increasing growth time was linear as shown in Figure 2(a). At 850 ^oC the deposition rate becomes slow, e.g. 30 minutes results in a thickness of 23 ± 3 nm. Higher growth temperatures also gave rise to a linear increase in thickness with increasing deposition time (not shown). Becker et al. previously reported an increase in deposition rate with deposition time in similar experiments[27]. However, this was with much shorter deposition times (~ 1s) and so is not directly comparable.

The deposition rate was seen to increase in an exponential fashion with increasing growth temperature as shown in Figure 2(b). This suggests a thermally activated process which can be described by the Arrhenius equation. A plot of the natural log of the deposition rate against the inverse of the deposition temperature as shown in Figure 2(c) verifies this. From the slope of this graph an activation energy of 2.68 ± 0.15 eV (259 ± 15 kJ/mol) was calculated. For comparison acetylene has an enthalpy of formation of 226.7 kJ/mol. This value is close to literature values[34], but it should be noted that there is little difference between this and the activation energy for PyC deposition from other similar sized hydrocarbons.

Varied growth pressures were also used to modulate the thickness of films. PyC films were grown at different growth pressures whilst keeping all other growth parameters constant (T = 950 ^{o}C, C_2H_2 flow = 180 sccm). The film thicknesses for different growth pressures are shown in Figure 2(d). The growth pressure was seen to have a big impact on film thickness with a pressure of 20 Torr giving a deposition rate of 13.32 ± 0.66 nm/min, 10 Torr giving a deposition rate of 2.49 ± 0.28 nm/min and 5 Torr giving a deposition rate of 0.61 ± 0.10 nm/min.

3.2 Surface Analysis

AFM analysis was used to probe the surface roughness and morphology of PyC films grown. AFM images were taken for different deposition times for T = 950 ^{o}C and P = 20 Torr, the image acquired for a deposition time of 10 minutes is shown in Figure 3(a). A line section giving a surface profile is shown in Figure 3(b), this shows a series of peaks and troughs, but the magnitude of these is such that the average surface roughness is calculated to be < 1 nm, implying very smooth films. A plot of average surface roughness as a function of deposition time is shown in Figure 3(b). Under these growth conditions the film roughness does not

increase with increasing film thickness and is always less than 1 nm. This is significantly smoother than conducting films produced from CNTs which typically have a roughness greater than 10 nm. It is well established that the nanotexture of PyC is dependent on the processing conditions used[38]. In this case, for higher growth temperatures and thus higher deposition rates the surface roughness is seen to increase and at very high temperatures (1050 ^{o}C and higher) globular structures with heights > 50 nm are seen to form (see supplementary information, S1). This observation is consistent with selected area electron diffraction (SAED) measurements performed by Meadows et al. who showed an increase in the isotropy of PyC with increasing deposition temperature[39]. The increased roughness can be attributed to the rapid nucleation of crystals (which occurs at higher temperatures). Thus, for smooth films, which are preferable for coatings, lower deposition temperatures are required. This smoothness is important for reliability, processability and interfacing of such films.

3.3 Electron Microscopy

Electron microscopy allowed for both short and long range investigation of the PyC/SiO_2 interface and also gave information on the crystallinity of the PyC grown. A low magnification image of the interface between a PyC film and its substrate is shown in Figure 4(a). This image outlines uniform coverage over a large area. A higher magnification SEM image of such a uniform coating is shown in Figure 4(b).

An HRTEM image of the cross sectional interface between PyC and the SiO_2 substrate is shown in Figure 4(c). From this a laminar like deposition is observed. Further information is garnered from a higher magnification image as shown in Figure 4(d). This allows for the crystallites to be directly viewed and suggests that domains are ~2 nm in size. It appears that there is preferential stretching of crystallites perpendicular to the <001> direction. A fast

Fourier transform (FFT) of the HRTEM image in this region was produced and an orientation angle of ≈ 46 ^{o} was observed implying that the PyC is highly textured[40].

3.4 Spectroscopic Characterisation

The composition and crystallinity of PyC films was investigated using a combination of Raman spectroscopy and XPS. Raman spectroscopy is a powerful tool for investigating different allotropes of carbon and has traditionally been used for characterisation of graphite[41], diamond[42] and amorphous carbon materials[43] as well as CNTs[44, 45] and graphene[46] in recent years. The main features in the spectra of graphitic materials are *D, G* and *2D* bands at ~1330 cm^{-1}, ~1580 cm^{-1} and ~2700 cm^{-1} respectively. The *G* band stems from in plane vibrations and has E_{2g} symmetry; this is observed in all sp^2 carbon systems. In graphite the *G* band can be fitted with a single Lorentzian peak and can be assigned to an in-plane tangential optical phonon. The *D* band stems from a double resonance process involving a phonon and a defect and can be considered as a breathing mode of A_{1g} symmetry. Structural defects (such as edges, vacancies or dopants) are generally the cause of the *D* band and as such its relative intensity can be related to the average crystallite size[41]. The *2D* band is an overtone of the *D* band. Like the *D* band it stems from a double resonance process[47]. However, it does not require a defect for activation and instead involves scattering from a second phonon and so its intensity can be related to spatial uniformity in the graphitic plane or the uniformity of interlayer spacing.

Comparative spectra of PyC and graphite powder (Sigma Aldrich) are shown in Figure 5(a). The PyC film has a large *D* band contribution and broadened *D* and *G* bands when compared with the graphite powder, which is indicative of its nanocrystalline nature[41, 48]. Furthermore, the *2D* band is suppressed, forming a broad bump, thus implying a lack of spatial uniformity, or that the PyC is laminar in nature[49]. The spectra for PyC films grown

under different growth conditions showed little change in the *G* and *D* band shape or intensity ratios suggesting the disorder levels and crystallite size were similar. This implies that the growth mechanism in the given temperature range is analogous (see supplementary information, S2).

Additional information was obtained by following the peak fitting procedure outlined by Vallerot et al.[50]. This entailed the fitting of additional bands associated with nanocrystalline graphitic materials as well as the standard *D* and *G* bands. These additional bands are labelled *D', I* and *D''*. The *D'* band is known to occur in defective graphitic systems and manifests as a shoulder on the *G* band at ~ 1620 cm^{-1}[47]. The *I* band has been linked with disorder in the graphitic lattice, sp^2-sp^3 bonds[51] or the presence of polyenes[52] and is seen at ~ 1180 cm^{-1} whereas the *D''* band is generally thought to stem from the presence of amorphous carbon[53] and is seen at ~ 1500 cm^{-1}. The *I* and *D''* bands were fitted with Gaussian functions and the *D*, *G* and *D'* were fitted with Lorentzian functions. A deconvoluted plot is shown in Figure 5(b). An estimate of the crystallite size (L_a) of < 10 nm was obtained using the method of Cancado et al[48]. This fitting indicates that the films grown consisted of nanocrystalline graphitic domains giving rise to a highly disordered signal. The strong intensity of the *D''* band indicates significant contributions from amorphous carbon.

XPS was used to probe the surface of thin (~ 20 nm) PyC films grown at 950 ^oC. A wide scan of these films is shown in Figure 6(a). Traces of O, N and F species are seen. It is likely that these stem from contaminants incorporated during or after the growth process. Deconvolution of the C_{1s} spectrum is shown in Figure 6(b). The main peak is asymmetric and centred at 284.14 eV. This has a tail which extends into the higher energy region. This peak is indicative of polyaromatic or graphitic structures with sp^2 hybridisation and delocalised π electrons. The asymmetry is associated with metallic systems and gives a good indication of

conductivity [54, 55]. The peak was fitted with a Doniac-Sunjic function which best reproduces the asymmetry on the higher energy side[56]. This fitting contains a term α which is referred to as the asymmetry factor and gives a measure of the asymmetry observed.

The asymmetry factor α can be thought of as a measure of the screening of the core hole which depends on the delocalisation of the valence band. Highly defective (or nanocrystalline) graphitic systems display large asymmetry factors as they have a high density of edges and defect sites which leads to differential charging and the creation of excitonic states[57]. Highly crystalline graphitic materials have a higher delocalisation of electrons and so display a smaller asymmetry factor. Thus, the magnitude of α gives an indication of the in-plane order and level of defects in the graphitic lattice and in turn the electrical conductivity. Fitting the PyC C_{1s} spectrum gave an extrapolated value for α of 0.191 which is in good agreement with literature values[57]. Peak fitting of the C_{1s} level also indicated the presence of aliphatic species (284.67eV) and assorted functional groups, C-OH (285.8 eV), C-CF & C-N (286.82 eV), CF-C (288.1 eV) and COOH/COOR (288.79 eV) [54, 55, 58-60]. Of particular interest is the peak seen at 283.73 eV which is associated with extensive carbon doping of SiO_2. The combination of this peak and the position of the Si2p peak (101.5 eV, see supplementary information S3) suggests the presence of SiOC:H [61-63]. This is a highly porous low κ dielectric material. It is proposed that a thin layer is formed due to the dissolution of carbon in the SiO_2 substrate. Additional experiments and analysis are required to investigate the formation of this layer further.

3.5 Electrical Characterisation

The sheet resistance of PyC films was measured using the four point probe technique. Typically ten sites near the centre of each sample were measured. The sheet resistance as a

function of deposition time obtained at 950 ^{o}C and 20 Torr are shown in Figure 7. For clarity, the corresponding thickness measurements are included on the graph.

Using the thickness values obtained from profilometry and the sheet resistances measured by the four point probe technique the resistivity (ρ) could be calculated using the equation;

$$\rho = R_s t \qquad \text{eq. (1)}$$

The calculated value for PyC films produced at 950 ^{o}C and 20 Torr with 30 mins deposition was (2.02 ± 0.28) × 10^{-5} Ωm. Deposition times of 10 minutes and greater gave rise to similar resistivities (see inset on Figure 3). For deposition times less than 10 minutes (t < 50 nm) the resistivity was seen to increase suggesting a lack in uniformity for very thin films.

The measured value of ρ for films of thickness > 100 nm is larger than that of in-plane graphite[64] (1.4 × 10^{-5} Ωm), the best reported values for CNTs(~4 × 10^{-6} Ωm) [2] and CVD graphene films (10^{-7}-10^{-8} Ωm) [9] but is very close to that of reduced graphene oxide films(~1.8 × 10^{-5} Ωm) [65] and is less than that of pyrolysed photoresist films (PPF) (6.25 × 10^{-5} Ωm) [66] or liquid phase graphene based thin films(6.67 × 10^{-5} Ωm)[67]. This is in agreement with previous reports on PyC based vias and wires where it has been shown that PyC can carry high current densities[21] without suffering from size effects[22].

3.6 Transmittance Studies

For transparent electrode materials, a combination of high electrical conductivity and high optical transmittance is required. In practice, a combination of 90% transmittance in the visible range and a sheet resistance of < 200 Ω/square is generally thought to be the minimum industry standard[68]. To examine the suitability of different materials for this purpose it is convenient to use a figure of merit given by the ratio of the DC electrical conductivity (σ_{DC}) to the optical conductivity (σ_{op}). The DC electrical conductivity governs the response of

electrons to constant applied fields whereas the optical conductivity governs the response of electrons to optical fields. The optical conductivity is related to the absorption coefficient, α, by $\sigma_{op} \approx 2\alpha/Z_0$, [69, 70] where Z_0 is the impedance of free space (377 Ω).

Industry standard transparent conductors require a minimum conductivity ratio value of 35 for top end applications. For films whose transmittance (T) and sheet resistance (R_s) are known the conductivity ratio can be calculated using the equation;

$$T = \left(1 + \frac{Z_0}{2R_S}\frac{\sigma_{op}}{\sigma_{DC}}\right)^{-2} \qquad \text{eq. (2)}$$

A series of PyC samples were grown on fused quartz substrates (pure SiO_2, no underlying Si) with different growth times in order to measure transmittance of films of different thicknesses. Growth conditions involved a temperature of 950 ^{o}C and a pressure of 20 Torr. Representative absorbance spectra for different deposition times are shown in Figure 8(a). These show an increase in absorbance in the visible range with increasing film thickness. A peak in the absorbance is seen in the UV region at ~ 255 nm. This corresponds to an energy of ~4.86 eV. This peak is seen in a wide variety of graphite like materials and is assigned to interband absorption between π bands near the M point in the Brillouin zone[71].

The transmittance at 550 nm was shown to be 93 % for a deposition time of 2 minutes and < 1 % for 15 minutes deposition. Transmission values were compared with the sheet resistances for an extended series of different deposition times as shown in Figure 8(b). Using Equation 1, values in the range 0.8 – 1.1 were obtained for the conductivity ratio of PyC films. This value is superior to that of the majority of graphene films produced by liquid phase processing(0.001 – 0.7)[72], or reduced graphene oxide (0.42)[65] but below that of the best reported SWNT networks (13.0)[2] and Ag nanowire networks (500)[73]. However, it is important to note that PyC can be produced very cheaply with high throughput and high reproducibility. Furthermore, conformal coating is possible. These are major advantages over

films which are composed of ex-situ produced nano entities such as CNTs and graphene. Thus for applications which do not require a very low resistivity or a very high optical transmittance, such as electrodes in ICT and energy applications, PyC films may prove to be good competitors.

3.7 Electrochemical Characterisation

Electrochemical characterisation of PyC films was carried out using a ferro / ferricyanide redox probe which is commonly used for investigating carbon systems. A Cyclic voltammogram of an as grown film in 1 mM ferro / ferricyanide solution in 1 M KCl at a scan rate of 100 mV/s is shown in Figure 9(a) (black line). This has a large peak separation (~450 mV) and poorly defined peaks indicative of slow electron transfer.

Improved performance of such electrodes has previously been reported by Keeley et al. through the use of facile O_2 plasma treatments [37]. Similar results were obtained here for O_2 and N_2 plasma treatments and are shown in Figure 9(a). The redox peaks become well defined and have a reduced peak separation following treatments indicating a significant enhancement of the electron transfer rate. Electrochemical impedance spectroscopy further demonstrated the improvement in the electrochemical properties. A reduction in the size of the semi-circular region in the Nyquist plot (Figure 9(b)) was observed indicating a reduced resistance to charge transfer. This suggests diffusion control at moderate frequencies in the case of treated electrodes. The impressive properties and ease of functionalisation of these treated films makes them a strong candidate for replacing more expensive purpose synthesised carbon electrodes. Furthermore, the conformal deposition afforded by PyC CVD makes the coating of porous materials possible, opening a pathway for the production of high surface area electrodes.

4. Summary

Thin films of PyC were grown on SiO_2 substrates by CVD. The thickness and roughness of these films could be controlled by varying the temperature, pressure and deposition time used. AFM analysis showed that smooth films could be produced ($R_a \approx 0.5$ nm) and Raman spectroscopy verified their nanocrystalline nature. HRTEM analysis indicated that the films were laminar in nature and implied a crystallite size of ~2 nm. XPS spectra had an asymmetric graphitic peak, indicative of good conductivity. Trace contributions from aliphatic species and assorted carbon based functionalities were also seen.

The films grown had a resistivity of ~ 2×10^{-5} Ωm and a conductivity ratio (σ_{DC}/σ_{op}) in the range 0.8 - 1.1. These values were better than those typically seen for thin films of PPF and liquid phase processed graphene but still fall short of the best reported SWNT and AgNW based films. However, the low cost, high reproducibility and robustness of PyC films make them an interesting candidate for thin film applications.

Electrochemical analysis indicated that the as grown films possessed a relatively inert surface with slow electron transfer. Through the use of plasma treatments the electron transfer was greatly enhanced. This ability to tune surface properties makes these films of potential interest for a wide array of applications including reliable and cheap electrodes for electrochemical usage.

Acknowledgements

This work was supported by Enterprise Ireland CCAN EI project (CC_/2008/0503.B), Science Foundation Ireland under the CSET scheme and Embark initiative under the IRCSET scheme. G. P. K. is grateful for funding received from IRCSET, co-funded by Marie Curie Actions under FP7.

References

[1] Dan B, Irvin GC, Pasquali M. Continuous and Scalable Fabrication of Transparent Conducting Carbon Nanotube Films. ACS Nano. 2009;3(4):835-43.

[2] Doherty EM, De S, Lyons PE, Shmeliov A, Nirmalraj PN, Scardaci V, et al. The spatial uniformity and electromechanical stability of transparent, conductive films of single walled nanotubes. Carbon. 2009;47(10):2466-73.

[3] Futaba DN, Hata K, Yamada T, Hiraoka T, Hayamizu Y, Kakudate Y, et al. Shape-engineerable and highly densely packed single-walled carbon nanotubes and their application as super-capacitor electrodes. Nature Materials. 2006 Dec;5(12):987-94.

[4] Cao Q, Rogers JA. Ultrathin Films of Single-Walled Carbon Nanotubes for Electronics and Sensors: A Review of Fundamental and Applied Aspects. Advanced Materials. 2009 Jan;21(1):29-53.

[5] Berger C, Song ZM, Li TB, Li XB, Ogbazghi AY, Feng R, et al. Ultrathin epitaxial graphite: 2D electron gas properties and a route toward graphene-based nanoelectronics. Journal of Physical Chemistry B. 2004 Dec;108(52):19912-6.

[6] Hamilton CE, Lomeda JR, Sun ZZ, Tour JM, Barron AR. High-Yield Organic Dispersions of Unfunctionalized Graphene. Nano Letters. 2009 Oct;9(10):3460-2.

[7] Hernandez Y, Nicolosi V, Lotya M, Blighe FM, Sun ZY, De S, et al. High-yield production of graphene by liquid-phase exfoliation of graphite. Nature Nanotechnology. 2008;3(9):563-8.

[8] Lotya M, Hernandez Y, King PJ, Smith RJ, Nicolosi V, Karlsson LS, et al. Liquid Phase Production of Graphene by Exfoliation of Graphite in Surfactant/Water Solutions. Journal of the American Chemical Society. 2009;131(10):3611-20.

[9] Bae S, Kim H, Lee Y, Xu X, Park J-S, Zheng Y, et al. Roll-to-roll production of 30-inch graphene films for transparent electrodes. Nat Nano. 2010;5(8):574-8.

[10] Kumar S, McEvoy N, Lutz T, Keeley GP, Nicolosi V, Murray CP, et al. Gas phase controlled deposition of high quality large-area graphene films. Chem Commun. 2010;46(9):1422-4.

[11] Li X, Cai W, An J, Kim S, Nah J, Yang D, et al. Large-Area Synthesis of High-Quality and Uniform Graphene Films on Copper Foils. Science. 2009 June 5, 2009;324(5932):1312-4.

[12] Koster A, Matzner HD, Nicholsi DR. PBMR design for the future. Nuclear Engineering and Design. 2003;222(2-3):231-45.

[13] Leomand GC, inventor Societe Nationale Industrielle Aerospatiale (Paris, FR), assignee. Pyrolytic Carbon Nose for Hypersonic Vehicles. United States. 1973.

[14] Wen C-Y, Huang G-W. Application of a thermally conductive pyrolytic graphite sheet to thermal management of a PEM fuel cell. Journal of Power Sources. 2008;178(1):132-40.

[15] Bruckmann H, Huttinger KJ. Carbon, A promising Material in endoprosthetics 1. The Carbon Materials and Their Mechanical Properties. Biomaterials. 1980;1(2):67-72.

[16] Pesakova V, Klezl Z, Balik K, Adam M. Biomechanical and biological properties of the implant material carbon-carbon composite covered with pyrolytic carbon. J Mater Sci-Mater Med. 2000 Dec;11(12):793-8.

[17] Reznik B, Gerthsen D, Hüttinger KJ. Micro- and nanostructure of the carbon matrix of infiltrated carbon fiber felts. Carbon. 2001;39(2):215-29.

[18] Zhang WG, Hu ZJ, Hüttinger KJ. Chemical vapor infiltration of carbon fiber felt: optimization of densification and carbon microstructure. Carbon. 2002;40(14):2529-45.

[19] Allouche H, Monthioux M, Jacobsen RL. Chemical vapor deposition of pyrolytic carbon on carbon nanotubes: Part 1. Synthesis and morphology. Carbon. 2003;41(15):2897-912.

[20] Taylor CA, Chiu WKS. Characterization of CVD carbon films for hermetic optical fiber coatings. Surface and Coatings Technology. 2003;168(1):1-11.

[21] Aichmayr G, Avellan A, Duesberg GS, Kreupl F, Kudelka S, Liebau M. Carbon / high-k Trench Capacitor for the 40nm DRAM Generation. VLSI Technology, 2007 IEEE Symposium on; 2007; 2007. p. 186-7.

[22] Graham AP, Schindler G, Duesberg GS, Lutz T, Weber W. An investigation of the electrical properties of pyrolytic carbon in reduced dimensions: Vias and wires. Journal of Applied Physics. 2010;107(11):114316.

[23] Raghavan G, Hoyt JL, Gibbons JF. Polycrystalline Carbon - A Novel Material for Gate Electrodes in MOS Technology. Jpn J Appl Phys Part 1 - Regul Pap Short Notes Rev Pap. 1993 Jan;32(1B):380-3.

[24] Graham AP, Richter K, Jay T, Weber W, Knebel S, Schroder U, et al. An investigation of the electrical properties of metal-insulator-silicon capacitors with pyrolytic carbon electrodes. Journal of Applied Physics. 2010 Nov;108(10).

[25] Kreupl F. Carbon-based Materials as Key-enabler for "More Than Moore". MRS Online Proceedings Library. 2011;1303.

[26] Borodina LM, Tesner PA. Kinetics of formation of pyrocarbon from acetylene. Solid Fuel Chem. 1983;17(4):152-4.

[27] Becker A, Huttinger KJ. Chemistry and kinetics of chemical vapor deposition of pyrocarbon - II - Pyrocarbon deposition from ethylene, acetylene and 1,3-butadiene in the low temperature regime. Carbon. 1998;36(3):177-99.

[28] Becker A, Huttinger KJ. Chemistry and kinetics of chemical vapor deposition of pyrocarbon - III - Pyrocarbon deposition from propylene and benzene in the low temperature regime. Carbon. 1998;36(3):201-11.

[29] Becker A, Huttinger KJ. Chemistry and kinetics of chemical vapor deposition of pyrocarbon - IV - Pyrocarbon deposition from methane in the low temperature regime. Carbon. 1998;36(3):213-24.

[30] Becker A, Huttinger KJ. Chemistry and kinetics of chemical vapor deposition of pyrocarbon - V - Influence of reactor volume/deposition surface area ratio. Carbon. 1998;36(3):225-32.

[31] Benzinger W, Becker A, Huttinger KJ. Chemistry and kinetics of chemical vapour deposition of pyrocarbon .1. Fundamentals of kinetics and chemical reaction engineering. Carbon. 1996;34(8):957-66.

[32] Ziegler I, Fournet R, Marquaire PM. Pyrolysis of propane for CVI of pyrocarbon - Part II. Experimental and modeling study of polyaromatic species. J Anal Appl Pyrolysis. 2005 Jun;73(2):231-47.

[33] Ziegler I, Fournet R, Marquaire PM. Pyrolysis of propane for CVI of pyrocarbon: Part I. Experimental and modeling study of the formation of toluene and aliphatic species. J Anal Appl Pyrolysis. 2005;73(2):212-30.

[34] Lacroix R, Fournet R, Ziegler-Devin I, Marquaire PM. Kinetic modeling of surface reactions involved in CVI of pyrocarbon obtained by propane pyrolysis. Carbon. 2010 Jan;48(1):132-44.

[35] Ziegler I, Fournet R, Marquaire PM. Influence of surface on chemical kinetic of pyrocarbon deposition obtained by propane pyrolysis. J Anal Appl Pyrolysis. 2005 Mar;73(1):107-15.

[36] Smits FM. Measurement of sheet resistivities with four-point probe. Bell System Technical Journal. 1958;37(3):711-8.

[37] Keeley GP, McEvoy N, Kumar S, Peltekis N, Mausser M, Duesberg GS. Thin film pyrolytic carbon electrodes: A new class of carbon electrode for electroanalytical sensing applications. Electrochemistry Communications. 2010 Aug;12(8):1034-6.

[38] Bourrat X, Langlais F, Chollon G, Vignoles GL. Low temperature pyrocarbons: A review. Journal of the Brazilian Chemical Society. 2006 Sep-Oct;17(6):1090-5.

[39] Meadows PJ, López-Honorato E, Xiao P. Fluidized bed chemical vapor deposition of pyrolytic carbon - II. Effect of deposition conditions on anisotropy. Carbon. 2009;47(1):251-62.

[40] López-Honorato E, Meadows PJ, Xiao P. Fluidized bed chemical vapor deposition of pyrolytic carbon – I. Effect of deposition conditions on microstructure. Carbon. 2009;47(2):396-410.

[41] Tuinstra F, Koenig JL. Raman Spectrum of Graphite. The Journal of Chemical Physics. 1970;53(3):1126-30.

[42] Nemanich RJ, Glass JT, Lucovsky G, Shroder RE. Raman scattering characterization of carbon bonding in diamond and diamond like thin films. J Vac Sci Technol A-Vac Surf Films. 1988 May-Jun;6(3):1783-7.

[43] Ferrari AC, Robertson J. Interpretation of Raman spectra of disordered and amorphous carbon. Physical Review B. 2000;61(20):14095.

[44] Duesberg GS, Blau WJ, Byrne HJ, Muster J, Burghard M, Roth S. Experimental observation of individual single-wall nanotube species by Raman microscopy. Chemical Physics Letters. 1999;310(1-2):8-14.

[45] Piscanec S, Lazzeri M, Robertson J, Ferrari AC, Mauri F. Optical phonons in carbon nanotubes: Kohn anomalies, Peierls distortions, and dynamic effects. Physical Review B. 2007 Jan;75(3).

[46] Ferrari AC, Meyer JC, Scardaci V, Casiraghi C, Lazzeri M, Mauri F, et al. Raman Spectrum of Graphene and Graphene Layers. Physical Review Letters. 2006;97(18):187401.

[47] Ferrari AC. Raman spectroscopy of graphene and graphite: Disorder, electron-phonon coupling, doping and nonadiabatic effects. Solid State Commun. 2007 Jul;143(1-2):47-57.

[48] Cancado LG, Takai K, Enoki T, Endo M, Kim YA, Mizusaki H, et al. General equation for the determination of the crystallite size L-a of nanographite by Raman spectroscopy. Applied Physics Letters. 2006 Apr;88(16).

[49] López-Honorato E, Meadows PJ, Shatwell RA, Xiao P. Characterization of the anisotropy of pyrolytic carbon by Raman spectroscopy. Carbon. 2010;48(3):881-90.

[50] Vallerot JM, Bourrat X, Mouchon A, Chollon G. Quantitative structural and textural assessment of laminar pyrocarbons through Raman spectroscopy, electron diffraction and few other techniques. Carbon. 2006 Aug;44(9):1833-44.

[51] Bacsa WS, Lannin JS, Pappas DL, Cuomo JJ. Raman scattering of laser-deposited amorphous carbon. Physical Review B. 1993;47(16):10931.

[52] Ishida H, Fukuda H, Katagiri G, Ishitani A. An Application of Surface-Enhanced Raman Scattering to the Surface Characterization of Carbon Materials. Appl Spectrosc. 1986;40(3):322-30.

[53] Jawhari T, Roid A, Casado J. Raman spectroscopic characterization of some commercially available carbon black materials. Carbon. 1995;33(11):1561-5.

[54] Darmstadt H, Roy C. Surface spectroscopic study of basic sites on carbon blacks. Carbon. 2003;41(13):2662-5.

[55] Dekanski A, Stevanovic J, Stevanovic R, Nikolic BZ, Jovanovic VM. Glassy carbon electrodes: I. Characterization and electrochemical activation. Carbon. 2001;39(8):1195-205.

[56] Doniach S, Sunjic M. Many-electron singularity in X-ray photoemission and X-ray line spectra from metals. Journal of Physics C: Solid State Physics. 1970;3(2):285.

[57] Cheung TTP. X-ray Photoemission of Carbon - Lineshape Analysis and Application to Studies of Coals. Journal of Applied Physics. 1982;53(10):6857-62.

[58] Carlo SR, Wagner AJ, Fairbrother DH. Iron Metalization of Fluorinated Organic Films: A Combined X-ray Photoelectron Spectroscopy and Atomic Force Microscopy Study. The Journal of Physical Chemistry B. 2000;104(28):6633-41.

[59] Desimoni E, Casella GI, Morone A, Salvi AM. XPS determination of oxygen-containing functional groups on carbon-fibre surfaces and the cleaning of these surfaces. Surface and Interface Analysis. 1990;15(10):627-34.

[60] Ilangovan G, Chandrasekara Pillai K. Electrochemical and XPS Characterization of Glassy Carbon Electrode Surface Effects on the Preparation of a Monomeric Molybdate(VI)-Modified Electrode. Langmuir. 1997;13(3):566-75.

[61] Eon D, et al. High density fluorocarbon plasma etching of methylsilsesquioxane SiOC(H) low- k material and SiC(H) etch stop layer: surface analyses and investigation of etch mechanisms. Journal of Physics D: Applied Physics. 2007;40(13):3951.

[62] Karakuscu A, Guider R, Pavesi L, Sorarù GD. White Luminescence from Sol–Gel-Derived SiOC Thin Films. Journal of the American Ceramic Society. 2009;92(12):2969-74.

[63] Tsukasa N, Keiichiro Y, Yasuhiro S, Sumio A. High-Speed Deposition of New Dielectric Film Having the Low Refractive Index for the Rewritable HD DVD Media. 2005: Optical Society of America; 2005. p. ThD5.

[64] Cohen ER, Lide, D.R., Trigg, G.L. AIP Physics Desk Reference. Springer. 2003:396.

[65] Wang X, Zhi L, Mullen K. Transparent, Conductive Graphene Electrodes for Dye-Sensitized Solar Cells. Nano Letters. 2007;8(1):323-7.

[66] Schreiber M, Lutz T, Keeley GP, Kumar S, Boese M, Krishnamurthy S, et al. Transparent ultrathin conducting carbon films. Applied Surface Science. 2010;256(21):6186-90.

[67] De S, King PJ, Lotya M, O'Neill A, Doherty EM, Hernandez Y, et al. Flexible, Transparent, Conducting Films of Randomly Stacked Graphene from Surfactant-Stabilized, Oxide-Free Graphene Dispersions. Small. 2010;6(3):458-64.

[68] De S, King PJ, Lyons PE, Khan U, Coleman JN. Size Effects and the Problem with Percolation in Nanostructured Transparent Conductors. ACS Nano. 2010;4(12):7064-72.

[69] Okpalugo TIT, Papakonstantinou P, Murphy H, McLaughlin J, Brown NMD. High resolution XPS characterization of chemical functionalised MWCNTs and SWCNTs. Carbon. 2005;43(1):153-61.

[70] Liu W, Dang T, Xiao Z, Li X, Zhu C, Wang X. Carbon nanosheets with catalyst-induced wrinkles formed by plasma-enhanced chemical-vapor deposition. Carbon. 2011;49(3):884-9.

[71] Zhang JM, Eklund PC. Optical transmission of graphite and potassium graphite intercalation compounds. Journal of Materials Research. 1987;2(Copyright 1988, IEE):858-63.

[72] De S, Coleman JN. Are There Fundamental Limitations on the Sheet Resistance and Transmittance of Thin Graphene Films? ACS Nano. 2010;4(5):2713-20.

[73] De S, Higgins TM, Lyons PE, Doherty EM, Nirmalraj PN, Blau WJ, et al. Silver Nanowire Networks as Flexible, Transparent, Conducting Films: Extremely High DC to Optical Conductivity Ratios. ACS Nano. 2009;3(7):1767-74.

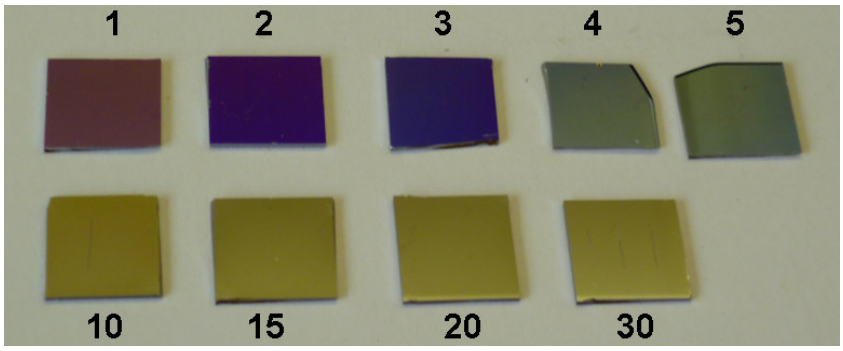

Figure 1 *Different thicknesses of PyC grown on SiO_2 substrates grown using different deposition times (numbers indicate deposition time in minutes) at $T = 950\,^{o}C$ and $P = 20$ Torr.*

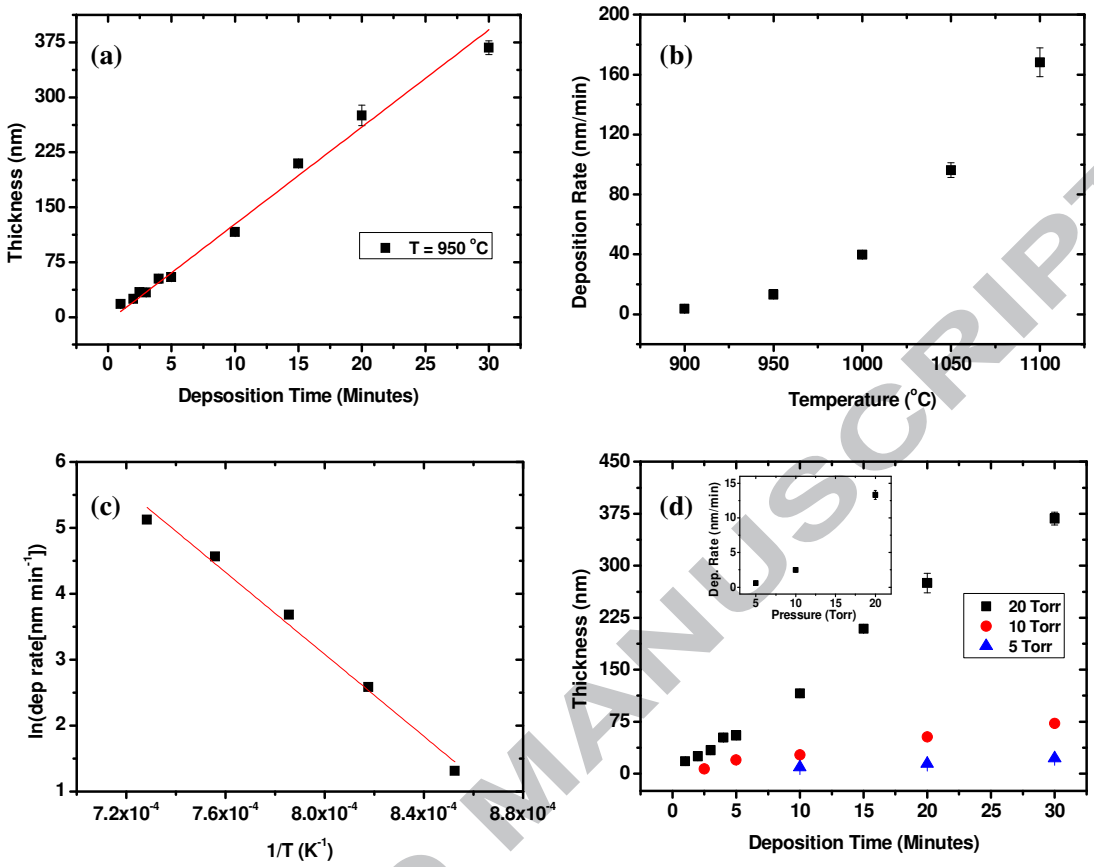

Figure 2 *(a) PyC film thickness as a function of deposition time at a growth temperature of 950 °C and a growth pressure of 20 Torr (b) Deposition rate as a function of temperature (c) Arrhenius plot, natural log of PyC deposition rate versus the reciprocal temperature. (d) PyC film thickness as a function of deposition time for different growth pressures at T = 950 °C. Inset: Deposition rate as a function of pressure.*

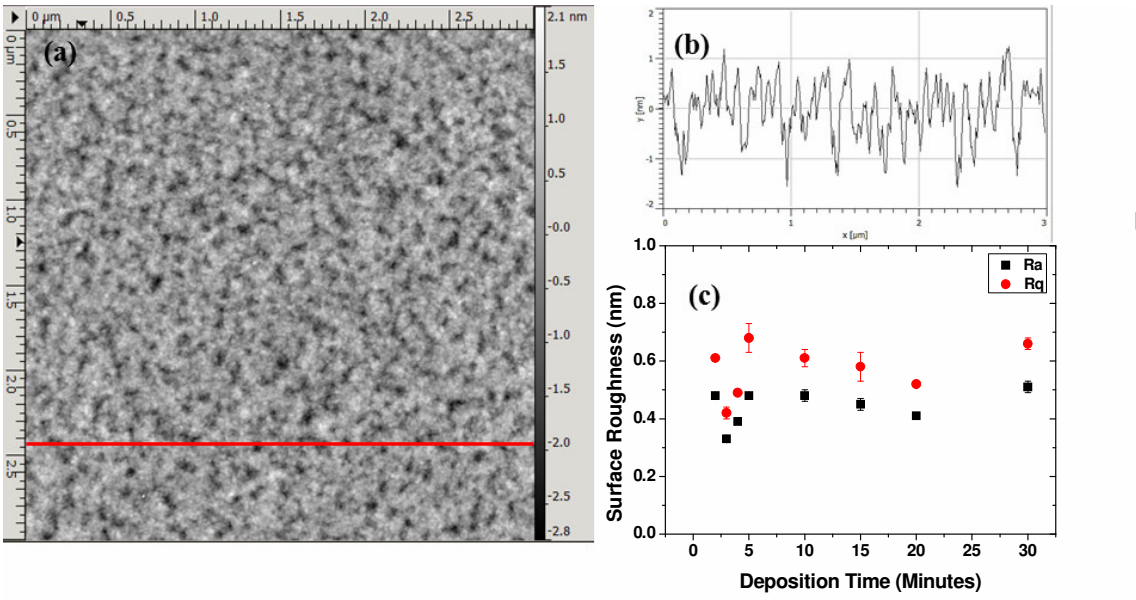

Figure 3 *(a) AFM image of PyC film with a deposition time of 10 minutes (scale, 3 x 3 μm). (b) Line section showing roughness of film (c) Arithmetic average (Ra) and root mean square (Rq) roughness values obtained by AFM for PyC films with different deposition times (all T = 950 ^{o}C, P = 20 Torr).*

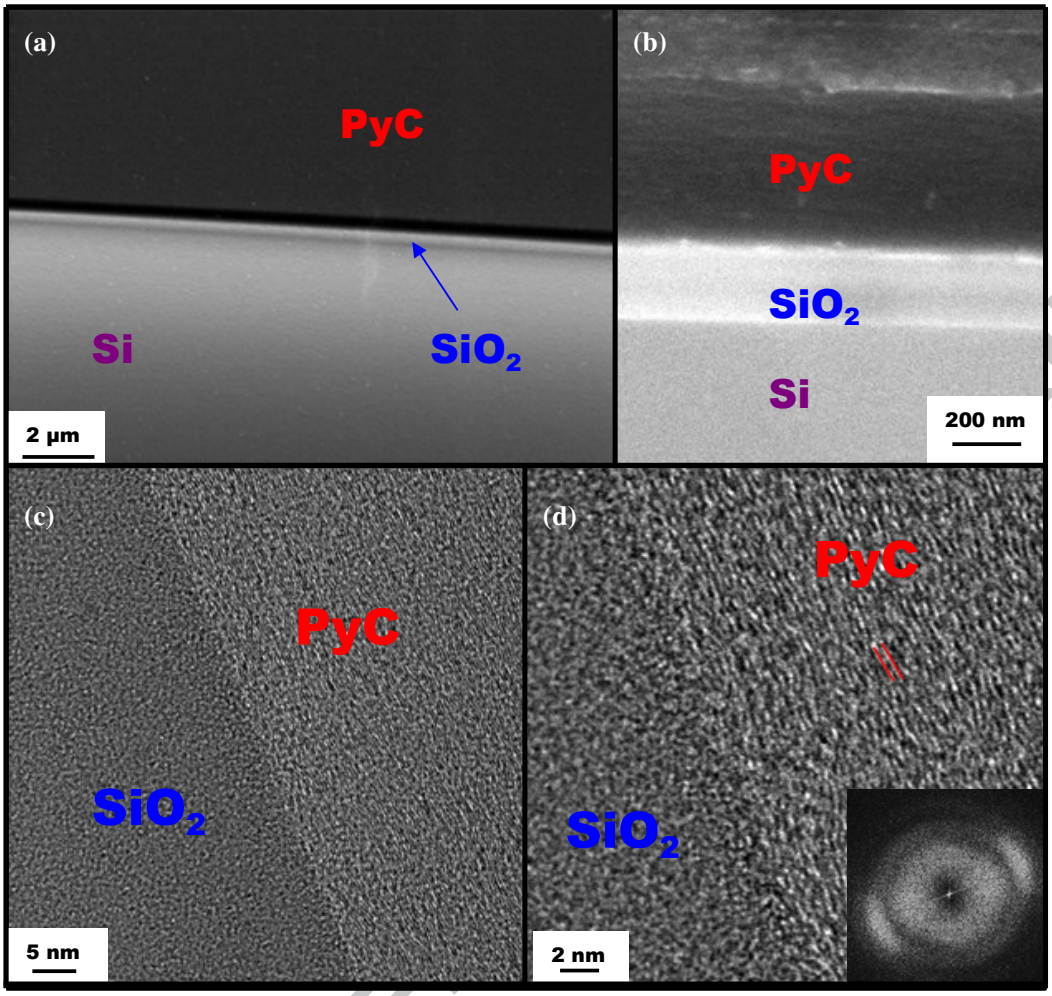

Figure 4 *Electron microscopy analysis of PyC samples (growth condition t = 15 mins, P = 20 Torr, T = 950 ^{o}C) (a) Low mag SEM image at 45^{o} tilt showing the interface between PyC and substrate (b) High mag SEM image showing interface between PyC and substrate (growth condition t = 30 mins, P = 20 Torr, T = 950 ^{o}C) (c) Low mag HRTEM image of the interface between PyC and the SiO_2 substrate. (d) HRTEM image of the interface between PyC and the SiO_2 substrate. The nanoscale texture of the PyC domains is evident. Inset: FFT of HRTEM image, an orientation angle of 46 ^{o} is observed.*

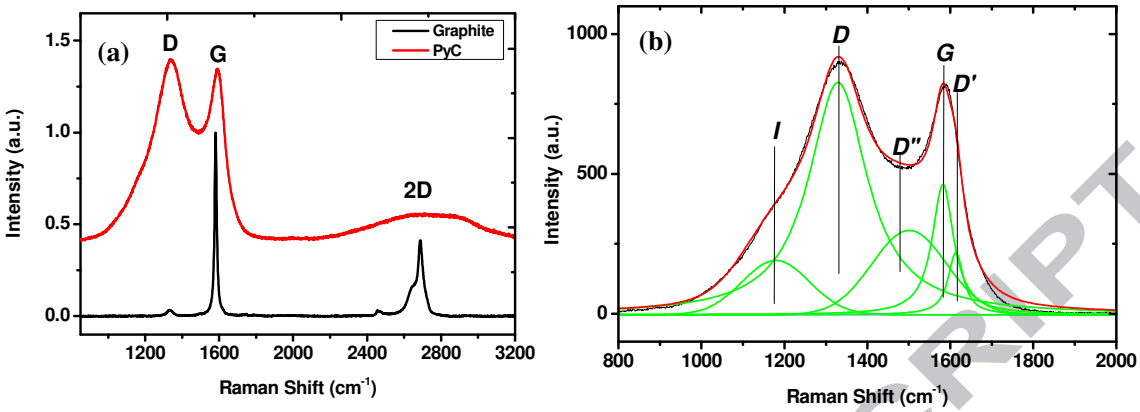

Figure 5 *(a) Raman spectra comparing PyC with graphite (b) Deconvoluted Raman spectrum of as grown PyC showing D, G, D', D'' and I bands.*

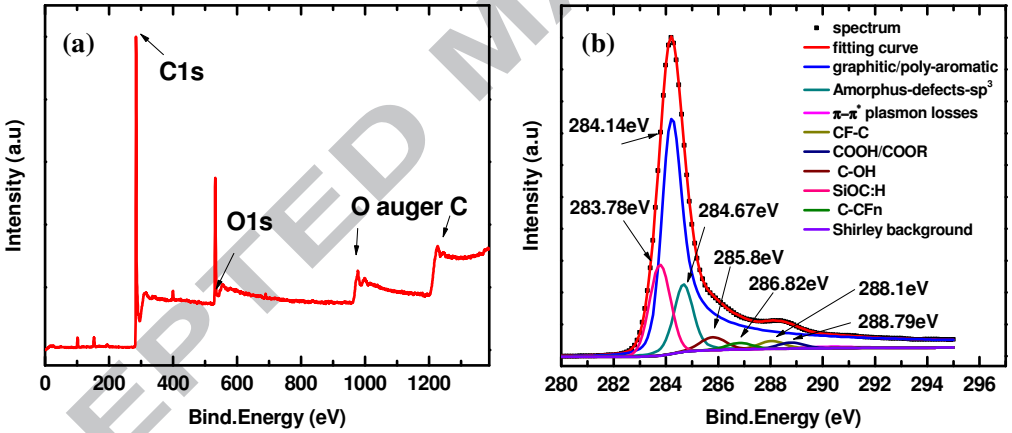

Figure 6 *XPS spectra for PyC films (a) Wide range scan and (b) Peak fitting of a high resolution C_{1s} core level spectrum for a PyC film grown at 950 ^{o}C.*

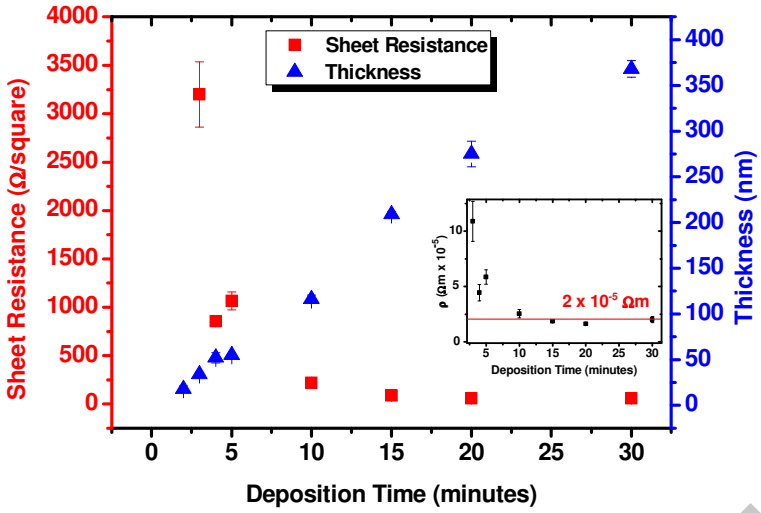

Figure 7 *Film thickness and sheet resistance as a function of deposition time for T = 950 ^{o}C and P = 20 Torr. Inset: Resistivity values for different deposition times.*

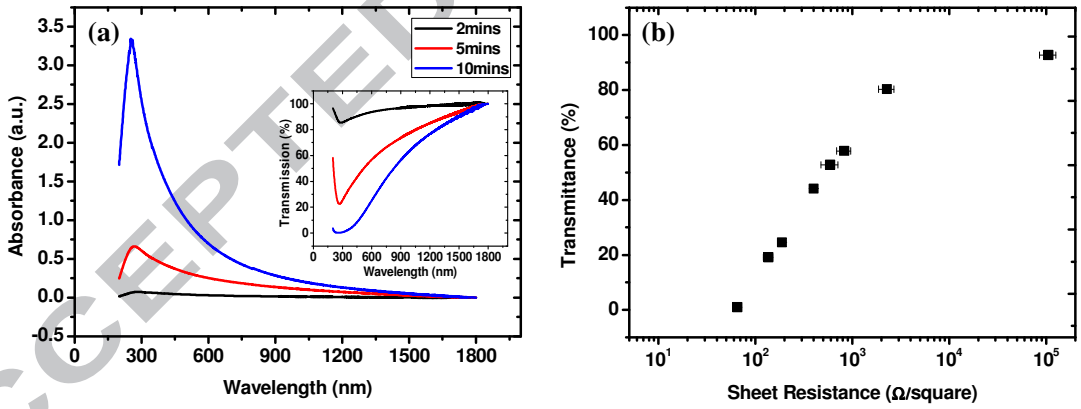

Figure 8 *(a) Absorbance spectra of PyC films grown on fused quartz substrates with different growth times. Inset: Transmittance in % for the same films (b) Sheet resistance versus transmittance for PyC films of different thickness*

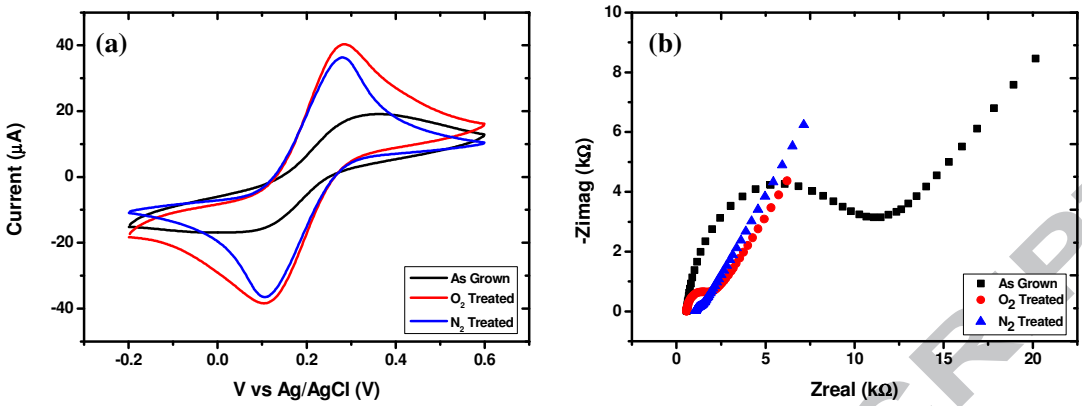

Figure 9 *(a) Cyclic Voltamograms obtained using PyC films as working electrodes in 1mM ferri / ferrocyanide in 1M KCl at a scan rate of 100 mV/s. (b) Corresponding Nyquist plots obtained at 0.26 V (vs. Ag / AgCl) with an AC voltage (10 mV) applied in the range 10^{-1}-10^{5} Hz. In each case a disc of radius 1.5 mm was exposed to the electrolyte.*